

# Synthesis, Crystal Structure, Kamlet-Taft and Catalan Solvatochromic Analysis of Novel Imidazole Derivatives

Jayaraman Jayabharathi · Venugopal Thanikachalam · Marimuthu Venkatesh Perumal · Natesan Srinivasan

Received: 11 May 2011 / Accepted: 13 September 2011 / Published online: 23 September 2011  
© Springer Science+Business Media, LLC 2011

**Abstract** Novel imidazole derivatives were synthesized and its crystal structure has been studied by single crystal XRD analysis. The photophysical properties of these imidazole derivatives were studied in several solvents, which include a wide range of apolar, polar and protic media. The observed lower fluorescence quantum yield may be due to an increase in the non-radiative deactivation rate constant. This is attributed to a loss of planarity in the excited state provided by the non coplanarity of the aryl rings attached to C(2) and N(1) atoms of the imidazole ring. Such a geometrical change in the excited state leads to an important Stokes shift, reducing the reabsorption and reemission effects in the detected emission in highly concentrated solutions. The highest fluorescence quantum yield of the imidazole derivatives are observed in polar media.

**Keywords** ORTEP · Imidazole · Laser · Catalan parameters · Aggregation

## Introduction

Recently, heterocyclic imidazole derivatives have attracted considerable attention because of their unique optical properties [1–3]. These compounds play very important role in chemistry as mediators for synthetic reactions, primarily for preparing functionalized materials [4–7]. Imidazole nucleus forms the main structure of some well-known components of human organisms and also has significant analytical applications such as laser [8], polymer stabilizer [9], Raman filters

[10] environmental probes in bio-molecules [11], etc. by utilizing their fluorescence and chemiluminescence properties.

Several factors contribute to the best laser performance of pyrromethene with respect to rhodamine as laser dye [12]: (1) low triplet-triplet absorption capacity at the lasing spectral region, which reduces the losses in the resonator cavity; (2) a poor tendency to self-aggregate in organic solvents, avoiding the fluorescence quenching of the monomer emission by the presence of aggregates in highly concentrated solutions, as was observed in rhodamine dyes: (3) and their high photostability [13–18], which improves the lifetime of the laser action with respect to that of rhodamines [19]. Owing to these properties, PM dyes have been successfully incorporated into different solid matrixes (polymers, silica, etc.) [20–22] to develop solid-state syntonizable dye lasers.

Photophysical properties and laser characteristics of compounds in liquid solutions and in polymeric matrixes [20–22], indicating that the laser behaviour is a consequence of the photophysical properties. Indeed, the evolution of the fluorescence wavelength and quantum yield with several environmental factors was similar to that observed for the laser band and efficiency, respectively. The Stokes shift modifies the lasing performance [23] in highly concentrated solutions because it affects the reabsorption and reemission phenomena, which shifts the emission band to longer wavelengths and reduces its efficiency [24]. In the present paper, the photophysical properties of imidazole derivatives **1** and **2** were investigated in a wide variety of solvents, including apolar, polar and protic solvents. The solvent effects on the absorption and fluorescence bands are analyzed by a multi-component linear regression in which several solvent parameters are simultaneously analyzed. The fluorescence quantum yield and the Stokes shift are analyzed to look for the best conditions to improve the lasing efficiencies of these derivatives.

J. Jayabharathi (✉) · V. Thanikachalam · M. Venkatesh Perumal · N. Srinivasan  
Department of Chemistry, Annamalai University,  
Annamalainagar 608 002 Tamilnadu, India  
e-mail: jtchalam2005@yahoo.co.in

## Experimental Section

### Materials and Methods

1,10-Phenanthroline-5,6-dione was synthesized and purified according to the reported literature procedure [25], benzaldehyde, 4-Fluorobenzaldehyde, aniline and all the other reagents were purchased from S.D. fine chemicals and used without further purification. The experimental procedure was used as same as described in our recent papers [26–34].

NMR spectra were recorded on a Bruker 400 MHz NMR instrument. UV–vis absorption and fluorescence spectra were recorded on Perkin Elmer spectrophotometer Lambda35 and Perkin Elmer LS55 spectrofluorimeter, respectively. Fluorescence spectra were corrected from the monochromator wavelength dependence and the photomultiplier sensibility. Fluorescence quantum yields ( $\phi$ ) were determined by means of the corrected fluorescence spectra of a dilute solution of imidazole derivatives in dichloromethane, using coumarin 47 in ethanol as a reference and by taking into account the solvent refractive index. Radiative decay curves were recorded by means of a time-correlated single-photon counting technique. Mass spectrum was recorded using Agilent 1100 Mass spectrometer.

The photophysical properties of the imidazole derivatives were recorded in dilute concentrations ( $1 \times 10^{-5}$  M). The fluorescence decay curves were analyzed as mono exponentials ( $X^2 < 1.2$ ), and the fluorescence decay time ( $\tau$ ) was obtained from the slope. The rate constant for the radiative ( $k_r$ ) and non-radiative ( $k_{nr}$ ) deactivation pathways were calculated to be:  $k_r = \Phi_p/\tau$ ,  $k_{nr} = 1/\tau - \Phi_p/\tau$  and  $\tau = (k_r + k_{nr})^{-1}$ .

### General Procedure for the Synthesis of the Imidazole Derivatives

The imidazole derivatives were synthesized from an unusual four components assembling of 1,10-Phenanthroline-5,6-dione, ammonium acetate, aniline and the corresponding benzaldehyde (Scheme 1). The reaction was monitored by

thin layer chromatography for the completion of the reaction. The reaction mixture was then extracted with dichloromethane and the resultant resinous material was purified by column chromatography using benzene:ethyl acetate (9:1) as the eluent.

### 1,2-Diphenyl-1H-imidazo[4,5-f][1,10]phenanthroline (1)

Yield: 55%. mp > 306 °C, Anal. calcd. for  $C_{25}H_{16}N_4$ : C, 80.63; H, 4.33; N, 15.04. Found: C, 79.95; H, 4.08; N, 14.98.  $^1H$  NMR (500 MHz,  $CDCl_3$ ):  $\delta$  7.22–7.38 (m, 5 H), 7.53–7.72 (m, 5H), 9.01 (d, 2 H, H-aryl,  $J=4.28$  Hz), 9.09 (d, 2H,  $J=7.68$  Hz), 9.17 (d, 2 H,  $J=2.16$  Hz).  $^{13}C$  (100 MHz,  $CDCl_3$ ):  $\delta$  119.62, 121.85, 123.30, 123.88, 126.65, 127.65, 128.20, 128.75, 129.11, 129.16, 129.75, 130.07, 130.31, 130.42, 136.05, 137.99, 144.20, 144.75, 147.67, 148.77, 151.88. MS: MS: m/z. 373 [M+1].

### 2-(4-Fluorophenyl)-1-phenyl-1H-imidazo[4,5-f][1,10]phenanthroline (2)

Yield: 55%. mp. 294 °C, Anal. calcd. for  $C_{25}H_{15}N_4F$ : C, 76.91; H, 3.87; N, 14.35. Found: C, 76.59; H, 3.68; N, 14.34.  $^1H$  NMR (500 MHz,  $CDCl_3$ ):  $\delta$  7.05 (t, 2H), 7.27 (q, 1H), 7.34 (m, 1H), 7.59 (m, 2H), 7.69 (m, 3H), 9.05 (d, 2H, H-aryl,  $J=4.4$  Hz), 9.08 (d, 2H,  $J=8.0$  Hz), 9.21 (d, 2H,  $J=2.8$  Hz).  $^{13}C$  (100 MHz,  $CDCl_3$ ):  $\delta$  115.55, 115.76, 119.77, 122.06, 123.54, 124.05, 126.87, 127.75, 129.02, 130.46, 130.55, 130.69, 131.31, 131.39, 136.27, 138.25, 144.55, 145.10, 147.95, 149.10, 151.07, 162.10, 164.60. MS: m/z. 390.9 [M+1], 391.9 [M+2].

### Computational Details

Quantum mechanical calculations were used to carry out the optimized geometry and HOMO-LUMO energies with Gaussian-03 program using the Becke3-Lee-Yang-Parr (B3LYP) functional supplemented with the standard 6–31G(d,p) basis set [35].

**Scheme 1** Synthesis of imidazole derivatives (1) and (2)

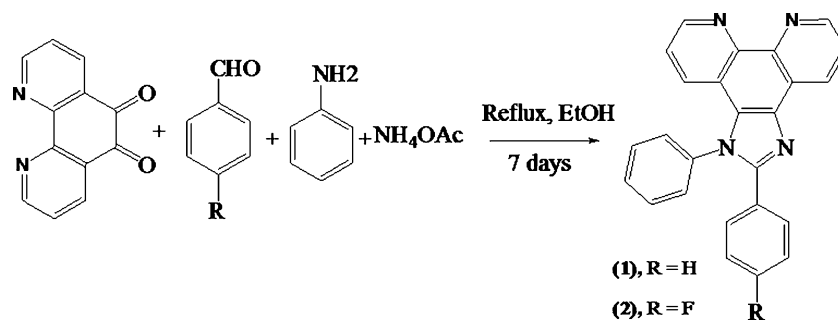


**Table 1** Photophysical data of the imidazole derivatives **1** and **2** in different solvents

solvent	Imidazole derivative ( <b>1</b> )							
	$\lambda_{ab}$ ( $\pm 0.1$ nm)	$\lambda_{fl}$ ( $\pm 0.4$ nm)	$\Delta\nu_{ss}$ ( $\text{cm}^{-1}$ )	$\Phi$ ( $\pm 0.05$ )	$\tau$ ( $\pm 0.01$ ns)	$\epsilon_{max}$ ( $10^4 \text{ M}^{-1} \text{ cm}^{-1}$ )	$K_r$ ( $10^8 \text{ s}^{-1}$ )	$k_{nr}$ ( $10^8 \text{ s}^{-1}$ )
Hexane	270.5	389.0	11261	0.35	4.13	3.58	0.85	1.57
Cyclohexane	272.0	392.4	11280	0.36	4.25	3.41	0.85	1.51
dioxane	268.1	394.5	11950	0.41	4.26	8.99	0.96	1.38
ethyl acetate	264.2	395.0	12533	0.45	4.30	6.49	1.05	1.28
Butanol	269.1	408.0	12651	0.48	4.43	7.36	1.08	1.17
Acetone	265.5	393.0	12219	0.45	4.35	7.21	1.03	1.26
ethanol	263.0	413.0	13809	0.49	4.08	5.40	1.20	1.25
methanol	265.0	415.0	13639	0.50	4.2	7.50	1.19	1.19
acetonitrile	263.8	397.0	12718	0.44	4.28	5.39	1.03	1.31
DMF	267.0	409.0	13003	0.41	4.71	7.69	0.87	1.25
ether	268.1	396.0	12046	0.40	4.28	4.12	0.93	1.40
THF	268.1	406.0	12668	0.42	4.22	4.21	1.00	1.37
1-propanol	267.3	409.0	12961	0.39	4.20	7.13	0.93	1.45

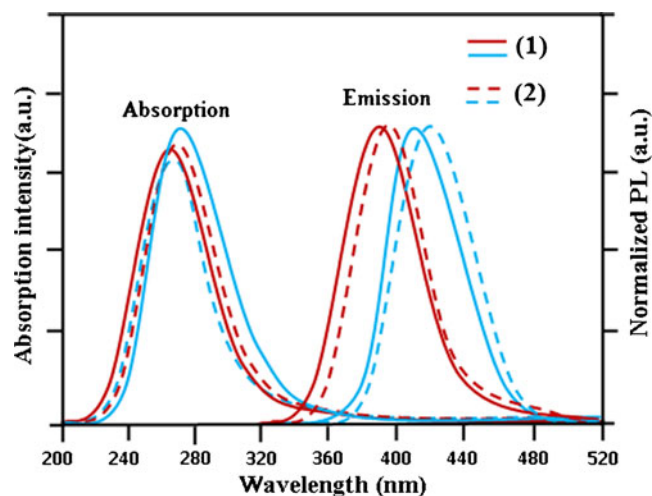
  

solvent	Imidazole derivative ( <b>2</b> )							
	$\lambda_{ab}$ ( $\pm 0.1$ nm)	$\lambda_{fl}$ ( $\pm 0.4$ nm)	$\Delta\nu_{ss}$ ( $\text{cm}^{-1}$ )	$\Phi$ ( $\pm 0.05$ )	$\tau$ ( $\pm 0.01$ ns)	$\epsilon_{max}$ ( $10^4 \text{ M}^{-1} \text{ cm}^{-1}$ )	$K_r$ ( $10^8 \text{ s}^{-1}$ )	$k_{nr}$ ( $10^8 \text{ s}^{-1}$ )
Hexane	267.5	394.0	12002	0.41	4.23	2.05	0.97	1.39
Cyclohexane	267.5	395.0	12066	0.42	4.21	2.03	1.00	1.38
dioxane	268.5	397.0	12055	0.43	4.34	3.56	0.99	1.31
ethyl acetate	268.8	398.0	12076	0.46	4.35	4.09	1.06	1.24
Butanol	269.4	411.0	12788	0.49	4.31	6.77	1.14	1.18
Acetone	268.6	400.0	12230	0.45	4.39	3.65	1.03	1.25
ethanol	268.5	416.0	13205	0.53	4.03	4.26	1.32	1.17
methanol	268.3	414.0	13117	0.54	4.35	3.93	1.24	1.06
acetonitrile	268.3	396.0	12019	0.48	4.38	4.10	1.10	1.19
DMF	268.5	412.0	12972	0.41	4.41	4.56	0.93	1.34
ether	268.4	398.0	12132	0.41	4.32	4.32	0.95	1.37
THF	268.0	409.0	12863	0.42	4.33	4.63	0.97	1.34
1-propanol	269.2	412.0	12875	0.41	4.51	6.23	0.91	1.31

## Results and Discussion

UV–vis absorption and fluorescence spectra (Table 1) of the imidazole derivatives **1** and **2** are shown in Fig. 1. In apolar solvents, the main absorption band is centered around 268 nm with a high molar absorption coefficient ( $\epsilon \approx 9 \times 10^4 \text{ M}^{-1} \text{ cm}^{-1}$ ), whereas the fluorescence spectrum is centered around 390 nm with a fluorescence quantum yield around 0.40. The fluorescence decay curve of **2**, which can be analyzed as a mono-exponential decay with a fluorescence lifetime of 4.2 ns.

The fluorescence spectrum of the imidazole derivative **2** is shifted to lower energies with respect to the parent compound **1** in common solvents. These spectral shifts are attributed to the higher inductive electron-acceptor character of the fluorine atom located at C(27) carbon atom. In the case of alcoholic solvents, bathochromic shifts were observed for both absorption and emission providing large



**Fig. 1** Absorption and fluorescence spectra of **1** (in bold lines) and **2** (in dotted lines) in hexane and ethanol

**Table 2** Selected Bond lengths, Bond angles and Torsional angles for the imidazole derivative (**1**)

Bond connectivity	Bond length (Å) <sup>a</sup>	Bond connectivity	Bond angle (°)	Bond connectivity	Torsional angle (°)
N1-C5	1.4020 (1.3840)	N1-C2-N3	111.6157 (112.63)	C4-C5-C6-C7	-179.3862 (-175.39)
N1-C18	1.4152 (1.4402)	N1-C5-C6	132.3707 (131.74)	N1-C5-C6-C7	0.4470 (0.8)
N1-C2	1.4222 (1.3752)	N1-C5-C4	105.9006 (105.14)	N3-C4-C5-C6	179.4411 (176.28)
C2-C24	1.4653 (1.4782)	N1-C18-C19	120.3840 (119.73)	C17-C4-C5-C6	-0.7134 (-3.5)
N3-C4	1.3966 (1.3789)	N1-C18-C23	120.2787 (118.93)	C2-N1-C5-C6	-2.8872 (-2.3)
N3-C2	1.3570 (1.3168)	C2-N1-C5	106.4092 (106.40)	C2-N1-C5-C6	-179.3215 (-175.82)
C4-C5	1.4292 (1.3770)	C2-C24-C25	121.0290 (121.16)	C5-N1-C18-C19	95.5898 (82.65)
C4-C17	1.4277 (1.4330)	C2-C24-C29	119.0361 (119.87)	C5-N1-C18-C23	-84.7810 (-98.62)
C5-C6	1.4270 (1.4321)	C2-C3-C4	105.7293 (104.52)	C5-N1-C2-N3	-0.4790 (-0.73)
N10-C11	1.3701 (1.3506)	N3-C4-C5	110.3424 (111.31)	C5-N1-C2-C24	-179.6887 (-179.76)
C18-C19	1.4102 (1.3840)	N3-C2-C24	124.5154 (124.59)	C2-N3-C4-C17	-179.7216 (-179.93)
C18-C23	1.4116 (1.3745)	N3-C4-C17	128.8832 (127.30)	C4-N3-C2-C24	180.0063 (179.25)
C24-C29	1.4018 (1.3860)	C4-C5-C6	121.7286 (123.04)	N1-C18-C19-C20	179.5595 (177.39)
C24-C25	1.3999 (1.3890)	C5-C4-C17	120.7742 (121.38)	N1-C18-C23-C22	-179.7109 (-176.22)
C27-H27	1.1000 (0.9500)	C5-N1-C18	127.4376 (128.80)	N1-C2-C24-C29	-135.6627 (-125.55)
		C24-C25-C26	119.8997 (120.44)	C18-N1-C2-N3	-176.9773 (-174.58)
		C24-C29-C28	119.7874 (120.30)	N3-C2-C24-C29	44.5636 (55.54)
				N1-C2-C24-C25	46.2322 (56.56)
				C2-C24-C29-C28	-178.6538 (-177.29)
				C2-N1-C18-C23	74.91 (73.81)
				C7-C6-C11-N10	0.0300 (0.6)
				C9-N10-C11-C6	-0.0252 (-0.1)
				C14-N13-C12-C17	-0.0146 (-3.2)

<sup>a</sup> values given in the brackets are corresponding to XRD values

R[F<sup>2</sup> > 2σ(F<sup>2</sup>)] = 0.042; wR(F<sup>2</sup>) = 0.117; R indices (all data) = 0.0458

Stokes shift. These results suggest an important geometrical rearrangement in the S<sub>1</sub> excited state and these observations are in good agreement with the literature report [36].

X-ray data of **1** (Table 2) reveal that the fused ring system is essentially planar and the R indices data are given in Table 2. The imidazole ring makes dihedral angles of 77.41° and 56.26° with the phenyl ring attached to N(1) nitrogen and phenyl ring attached to C(2) carbon, respectively. The dihedral angle between the two phenyl rings is 65.50° found in the crystal structure (Fig. 2). In order to eliminate the crystal packing effect in the solid state, the molecular geometry of **1** and **2**, was further examined by DFT calculation [DFT/B3LYP16–31G(d,p)] [35] to make necessary comparison on an equal state basis. The key twist (α) is used to indicate the twist of imidazole ring from the aromatic six-membered ring at C(2) (Fig. 3). It reveals that α twist is correlated with fluorescent property, the larger α twist, the more drops the fluorescence quantum yield. Such a clear correlation indicates the importance of co-planarity between the imidazole and the phenyl ring at C(2). This correlation can be ascribed to the conjugation rigidity.

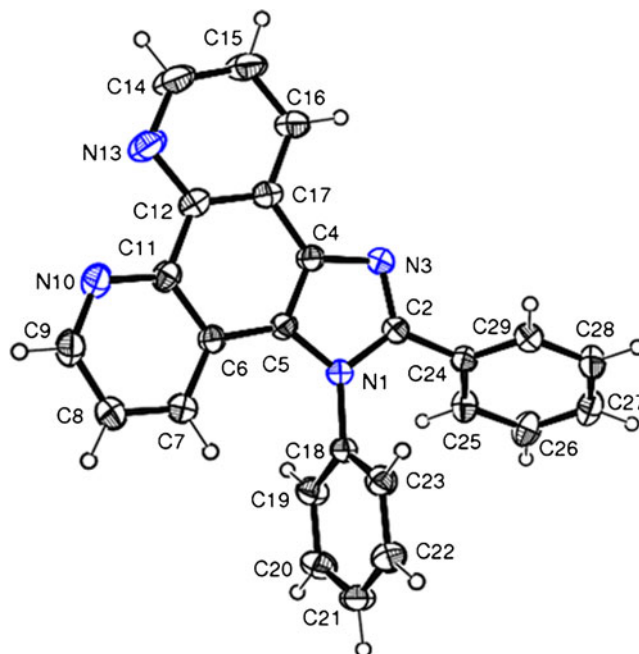


**Fig. 2** ORTEP diagram of 1,2-Diphenyl-1H-imidazo[4,5-f][1,10]phenanthroline (**1**)

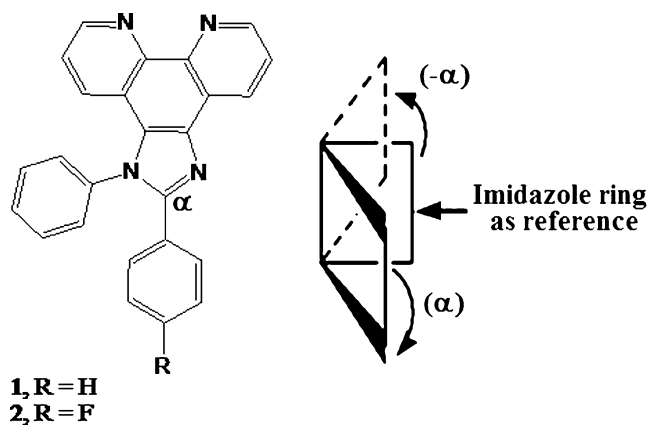


**Fig. 3** The key  $\alpha$  twist of imidazole ring at C(2)

When the two adjacent aromatic species are in a coplanar geometry, the  $p$ -orbitals from the C–C bond connecting the two species will have maximal overlapping and the two rings will have a rigid and delocalized conjugation, as the result, the bond is no longer a pure single bond, as evident from the X-ray data of **1**. When the two rings are deviated from each other, the  $p$ -orbital overlapping will be reduced. The partial conjugation will lead to less rigid structure; therefore, radiationless twist motion will deactivate the emitting state, leading to the low quantum yields (Table 1). Thus, it is suggested that fluorophores with the substitution at C(2) with a minimum loss of fluorescence property. All these XRD data are in good agreement with the theoretical values (Table 2). However, from the theoretical values it can be found that most of the optimized bond lengths, bond angles and dihedral angles are slightly higher than that of XRD values. These deviations can be attributed to the fact that the theoretical calculations were aimed at the isolated

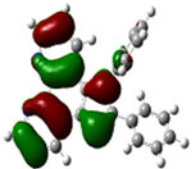
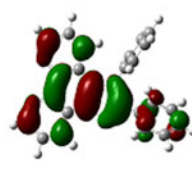
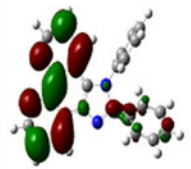
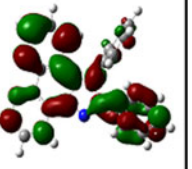
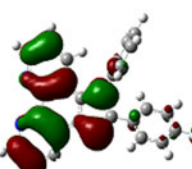
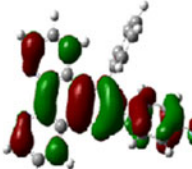
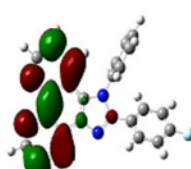
molecule in the gaseous phase whereas the XRD results were aimed at the molecule in the solid state.

The higher bathochromic shifts observed in the fluorescence band of the imidazole derivative **2** with respect to the parent imidazole derivative **1** can be interpreted by the Brunings-Corwin effect [37]. Because the distortion of the geometry in the excited state implies a decrease in the resonance energy, the fluorescence band is bathochromically shifted to a higher extent than the absorption band. Moreover, the loss of planarity in the excited state of the imidazole derivative could explain the lower fluorescence quantum yield in apolar solvents owing to an increase in the non-radiative processes.

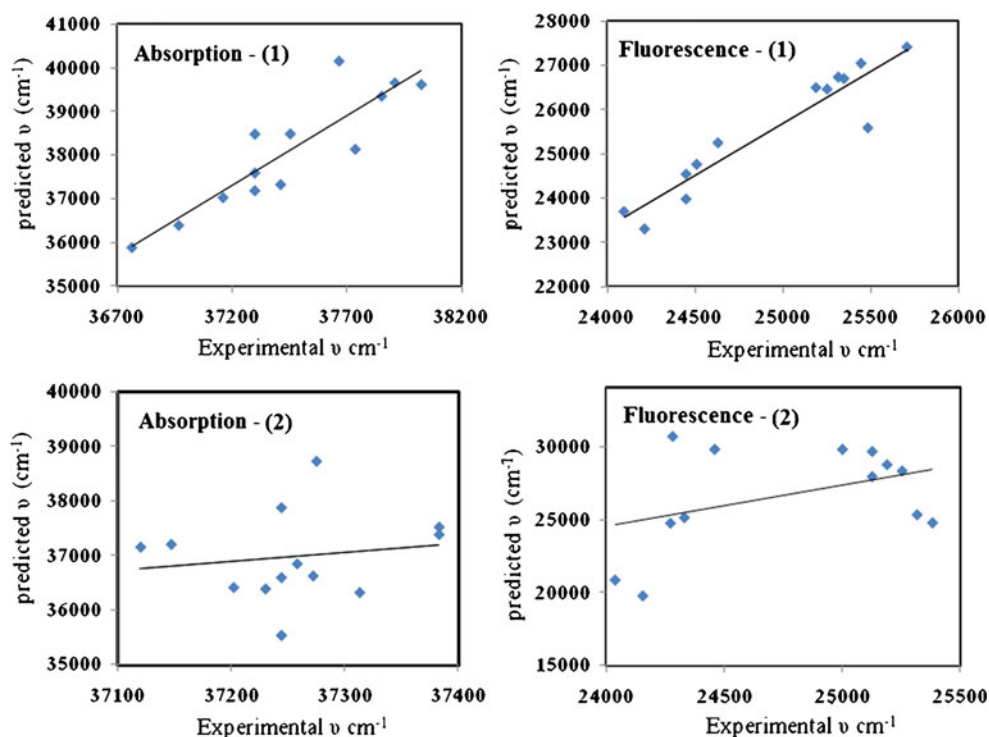
However, the shape of the absorption band is independent of the imidazole concentration suggesting the poor aggregation and it is a suitable behaviour in the performance of active media of lasers. Indeed, high concentration is necessary to bring about laser action, and the presence of aggregates could drastically reduce the fluorescence quantum yield owing to the efficient quenching of the monomer fluorescence by the aggregates [17]. However, experimental data indicate that the fluorescence band is shifted to lower energies by increasing the concentration. This bathochromic shift is attributed to reabsorption and reemission phenomena [38] and this result corroborates the importance of registering photophysical properties in dilute solutions.

Figure 4 shows the calculated contour maps for the electronic distribution of the HOMO and LUMO states by the B3LYP method. The electron density at position C(2) and the aryl ring attached to the C(2) carbon is augmented in the HOMO with respect to that in the LUMO state. Taking into account the resonance structures of the imidazole chromophore, we observed that the resonance structure “b” has the largest charge separation along the

**Fig. 4** HOMO-LUMO orbital picture of (1) and (2)

Compound	HOMO-1 (eV)	HOMO (eV)	LUMO (eV)	LUMO+1 (eV)
<b>1</b>	 E = -0.337	 E = -0.309	 E = -0.207	 E = -0.198
<b>2</b>	 E = -0.337	 E = -0.306	 E = -0.207	 E = -0.197

**Fig. 5** Correlation between the experimental absorption and fluorescence wavenumber with the predicted values obtained by a multicomponent linear regression using the  $\pi^*$ ,  $\alpha$  and  $\beta$ -scale (Taft) solvent parameters for (1) and (2)



short molecule axis. Consequently, its contribution would be more important in the  $S_0$  ground states than in the  $S_1$  excited states. Thus, the polar solvents would stabilize the  $S_0$  state more extensively than the  $S_1$  state, thereby increasing the energy gap between both states and explaining the solvatochromic shifts [39].

To analyze the solvatochromic effects, we have checked several methods [40–42]. Neither the absorption nor the fluorescence wavenumbers linearly correlate with the Lippert parameter  $\Delta f(\epsilon, n^2)$  [43], which considers the solvent polarity/polarizability or with the Reichardt parameter  $E_T^N(30)$  [41, 44], which takes into account several

**Table 3** Adjusted Coefficients ( $(\nu_x)_0$ ,  $c_a$ ,  $c_b$  and  $c_c$ ) and Correlation Coefficients ( $r$ ) for the Multilinear Regression Analysis of the Absorption  $\nu_{ab}$  and Fluorescence  $\nu_{fl}$  Wavenumbers and Stokes Shift

$(\nu_x)$	$(\nu_x)_0 \text{ cm}^{-1}$	$(\pi^*)$	$c_\alpha$	$c_\beta$	$r$
<b>Imidazole derivative (1)</b>					
$\lambda_{ab}$	$(3.69 \pm 0.022) \times 10^4$	$(4.46 \pm 2.516) \times 10^3$	$(8.72 \pm 7.266) \times 10^3$	$-(5.13 \pm 5.300) \times 10^3$	0.66
$\lambda_{fl}$	$(2.56 \pm 0.016) \times 10^4$	$(1.58 \pm 1.856) \times 10^3$	$-(7.71 \pm 5.359) \times 10^3$	$-(4.76 \pm 3.908) \times 10^3$	0.87
$\Delta \nu_{ss} = \nu_{ab} - \nu_{fl}$	$(1.13 \pm 0.031) \times 10^4$	$(2.87 \pm 3.524) \times 10^3$	$(1.02 \pm 1.177) \times 10^3$	$-(3.75 \pm 7.421) \times 10^3$	0.76
$(\nu_x)$	$(\nu_x)_0 \text{ cm}^{-1}$	$c_{SPP}^N$	$c_{SA}$	$c_{SB}$	$r$
$\lambda_{ab} \lambda_{fl}$	$(3.73 \pm 0.015) \times 10^4$	$(5.96 \pm 9.832) \times 10^3$	$(2.39 \pm 42.167) \times 10^3$	$-(2.51 \pm 43.459) \times 10^3$	0.64
$\Delta \nu_{ss} = \nu_{ab} - \nu_{fl}$	$(2.53 \pm 0.013) \times 10^4$	$-(10.93 \pm 8.674) \times 10^3$	$(35.87 \pm 37.198) \times 10^3$	$-(34.716 \pm 38.338) \times 10^3$	0.69
	$(1.21 \pm 0.022) \times 10^4$	$(16.89 \pm 14.273) \times 10^3$	$-(59.78 \pm 61.210) \times 10^3$	$-(59.839 \pm 6.386) \times 10^3$	0.56
<b>Imidazole derivative (2)</b>					
$\lambda_{ab}$	$(3.73 \pm 0.002) \times 10^4$	$-(1.22 \pm 0.261) \times 10^3$	$(3.14 \pm 0.786) \times 10^3$	$-(2.38 \pm 0.593) \times 10^3$	0.89
$\lambda_{fl}$	$(2.53 \pm 0.0113) \times 10^4$	$(5.00 \pm 1.443) \times 10^3$	$-(19.17 \pm 4.343) \times 10^3$	$-(13.81 \pm 3.277) \times 10^3$	0.92
$\Delta \nu_{ss} = \nu_{ab} - \nu_{fl}$	$(1.20 \pm 0.0129) \times 10^4$	$-(6.22 \pm 1.641) \times 10^3$	$(22.31 \pm 4.940) \times 10^3$	$-(16.19 \pm 3.727) \times 10^3$	0.89
$(\nu_x)$	$(\nu_x)_0 \text{ cm}^{-1}$	$c_{SPP}^N$	$c_{SA}$	$c_{SB}$	$r$
$\lambda_{ab}$	$(3.73 \pm 0.002) \times 10^4$	$-(1.59 \pm 1.620) \times 10^3$	$(4.75 \pm 6.950) \times 10^3$	$-(3.59 \pm 7.163) \times 10^3$	0.64
$\lambda_{fl}$	$(2.51 \pm 0.013) \times 10^4$	$-(5.47 \pm 8.842) \times 10^3$	$(11.87 \pm 37.919) \times 10^3$	$-(8.77 \pm 39.081) \times 10^3$	0.62
$\Delta \nu_{ss} = \nu_{ab} - \nu_{fl}$	$(1.22 \pm 0.013) \times 10^4$	$(3.88 \pm 8.759) \times 10^3$	$-(7.13 \pm 37.565) \times 10^3$	$-(5.21 \pm 38.716) \times 10^3$	0.58

( $\Delta \nu_{ss}$ ) of the imidazole derivative **1** and **2** with the Solvent Polarity/Polarizability, and the Acid and Base Capacity Using the Taft ( $\pi^*$ ,  $\alpha$  and  $\beta$ ) and the Catalan ( $SPP^N$ ,  $SA$  and  $SB$ ) Scales

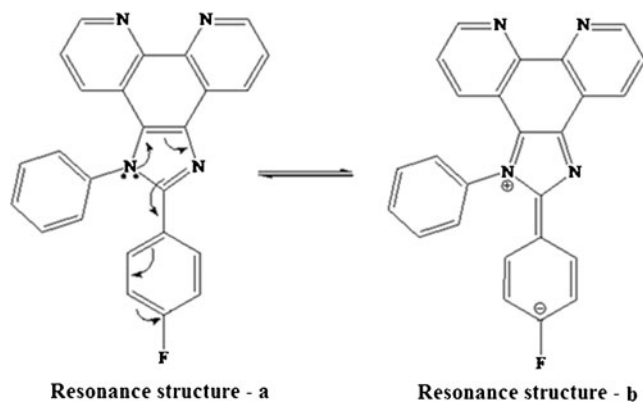


**Fig. 6** Resonance structures (a & b) of the imidazole chromophore (2)

solvent properties (polarity and H-bond donor capacity) in a common parameter. For these reasons, a multi-parameter correlation analysis is employed in which a physicochemical property is linearly correlated with several solvent parameters by means of Eq. 1:

$$(XYZ) = (XYZ)_0 + C_a A + C_b B + C_c C + \dots \quad (1)$$

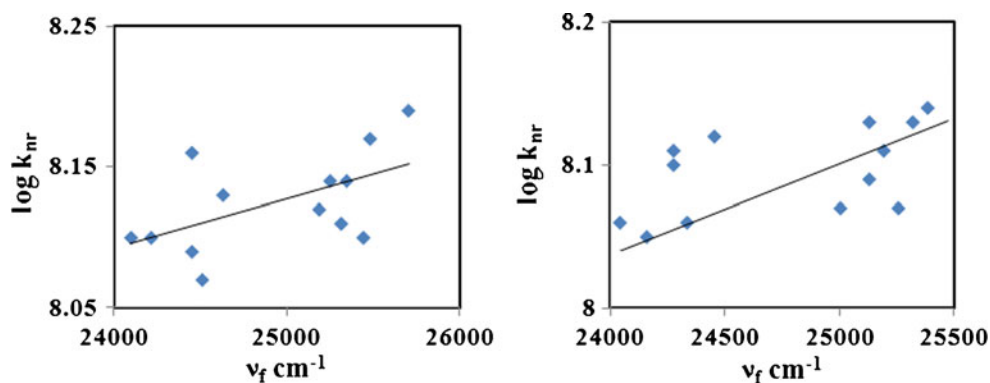
where  $(XYZ)_0$  is the physicochemical property in an inert solvent and  $C_a$ ,  $C_b$ ,  $C_c$  and so forth are the adjusted coefficients that reflect the dependence of the physicochemical property  $(XYZ)$  on several solvent properties. Solvent properties that mainly affect the photophysical properties of aromatic compounds are polarity, H-bond donor capacity and electron donor ability. Different scales for such parameters can be found in the literature, Taft et al. [45] propose the  $\pi^*$ ,  $\alpha$  and  $\beta$  scales, whereas more recently Catalan et al. [46] suggest the  $SPP^N$ , SA and SB scales to describe the polarity/polarizability, the acidity and basicity of the solvents respectively.

Figure 5 shows the obtained correlation between the absorption and fluorescence wavenumbers calculated by the multi-component linear regression employing the Taft-proposed solvent parameters and the experimental values are listed in Table 3. Table 3 lists the obtained adjustment

and correlation coefficients by the Taft and Catalan parameters. The dominant coefficient affecting the absorption and fluorescence bands of these imidazole derivatives **1** and **2** is that describing the polarity/polarizability of the solvent,  $C_{\pi^*}$  or  $C_{SPP}^N$  having a positive value, corroborating the above-mentioned solvatochromic shifts with the solvent polarity. The coefficient controlling the H-donor capacity or acidity of the solvent,  $C_\alpha$  or  $C_{SA}$ , is the lowest coefficient (Table 3), therefore, the solvent acidity does not play an important role in absorption and fluorescence displacements. The adjusted coefficient representing the electron releasing ability or basicity of the solvent,  $C_\beta$  or  $C_{SB}$  has a negative value, suggesting that the absorption and fluorescence bands shift to lower energies with the increasing electron-donating ability of the solvent. This effect can be interpreted in terms of the stabilization of the resonance structures of the chromophore (Fig. 6). Resonance structure “b” has the positive charge located at the nitrogen atom and it will be stabilized in basic solvents because this resonance structure is predominant in the  $S_1$  state, as discussed above and the stabilization of the  $S_1$  state with the solvent basicity would be more important than that of the  $S_0$  state. Consequently, the energy gap between the  $S_1$  and  $S_0$  states decreases and the absorption and fluorescence wavelengths shift to longer wavelengths with increasing solvent basicity.

However, the fluorescence quantum yield and lifetime values of imidazole derivatives were observed in common solvents. The solvent also affects the fluorescence quantum yield and lifetime of imidazole derivative and  $\phi$  and  $\tau$  values increase in polar/protic solvents (Table 1), although a general tendency in both parameters with respect to the solvent viscosity is not observed. These results indicate an extra non-radiative deactivation of imidazole derivative, which is not governed by the solvent viscosity. Figure 7 shows a correlation between the  $k_{nr}$  value and the fluorescence wave numbers of imidazole derivatives **1** and **2** by changing the nature of the solvent, indicating similar solvent parameters affecting both photophysical characteristics, as was also proposed for other aromatic systems [47–50].

**Fig. 7** Correlation between the rate constant of non-radiative deactivation ( $\log k_{nr}$ ) with the fluorescence wavenumbers of (1) and (2) in several solvents



It is well known that the flexibility/rigidity of the imidazole derivatives can control the mechanics of internal conversion. The flexibility/rigidity of the aromatic compounds can be analyzed in terms of the planarity of the  $\pi$ -electron system [51, 52]. This loss of planarity, especially in the excited state implies a less rigid structure and the excitation energy is more easily converted to vibrational energy and dissipated as heat, enhancing the internal conversion processes. Drexhage et al. [51] pointed out that the structure loosens up in some compounds upon excitation, enhancing the non-radiative deactivation processes. In the imidazole derivatives **1** and **2**, the steric hindrance between the aryl ring at N(1) of the imidazole ring and the aryl ring at C(2) of the imidazole, which makes the molecule in distorted way. Such a distortion from planarity leads to an augmentation of the non-radiative deactivation. Pavlopoulos et al. [13] also referred to the non-planarity of the chromophore provided by bulky substituents to explain the low fluorescence quantum yield.

The present photophysical characteristics of these imidazole derivatives would suggest a lower lasing efficiency because of its lower fluorescence quantum yield. However, high optical densities are required to produce laser signals and under these conditions, the losses at the resonator cavity by the reabsorption and reemission effects can be important. These imidazole derivatives are characterized by a higher Stokes shift which would reduce the losses at the resonator cavity by reabsorption and reemission effects, governed by the overlap between the absorption and emission spectra [30]. Therefore, the low fluorescence quantum yield to some extent can be compensated by its high Stokes shift and high laser efficiencies for imidazole derivatives [53–56]. Because the higher Stokes shift and highest fluorescence quantum yield of the imidazole derivative are recommended to achieve the highest laser efficiencies in liquid media.

## Conclusions

The presence of aryl rings at C(2) in the imidazole chromophore core originates a distortion from planarity in the imidazole units, mainly in the excited state, which leads to an increase in the rate constant of non-radiative deactivation and in the Stokes shift. Both photophysical factors have an opposite effect on the lasing efficiency. Thus, the increase in the loss of the resonator cavity due to the augmentation in the non-radiative processes could be compensated to some extent by a reduction in the reabsorption and reemission losses, owing to the high Stokes shift. From this photophysical studies, polar solvents are recommended to obtain the highest laser efficiencies in liquid media.

## References

- Santos J, Mintz EA, Zehnder O, Bosshard C, Bu XR, Gunter P (2001) New class of imidazoles incorporated with thiophenevinyl conjugation pathway for robust nonlinear optical chromophores. *Tetrahedron Lett* 42:805–808
- Hung WS, Lin JT, Chien CH, Tao YT, Sun SS, Wen YS (2004) Highly phosphorescent bis-cyclometallated iridium complexes containing benzoimidazole-based ligands. *Chem Mater* 16:2480–2488
- Chen CH, Shi J (1998) Metal chelates as emitting materials for organic electroluminescence. *Coord Chem Rev* 171:161–174
- Kamidate T, Yamaguchi K, Segawa T (1989) Lophine chemiluminescence for determination of chromium(VI) by continuous flow method. *Anal Sci* 5:429–433
- Nakashima K, Yamasaki H, Kuroda N, Akiyama S (1995) Evaluation of lophine derivatives as chemiluminogens by a flow-injection method. *Anal Chim Acta* 303:103–107
- MacDonald A, Chain KW, Nieman TA (1979) Lophine chemiluminescence for metal ion determinations. *Anal Chem* 51:2077–2082
- Marino DF, Ingle JD Jr (1981) Determination of chromium (VI) in water by lophine chemiluminescence. *Anal Chem* 53:294–298
- Chou PT, McMorrow D, Aartsma TJ, Kasha M (1984) The proton-transfer laser. Gain spectrum and amplification of spontaneous emission of 3-hydroxyflavone. *J Phys Chem* 88:4596–4599
- Keck J, Roessler M, Schroeder C, Stueber GJ, Waiblinger F, Stein M, Legourrierec D, Kramer HEA, Hoier H, Henkel S, Fischer P, Port H, Hirsch T, Tytz G, Hayoz P (1998) Ultraviolet absorbers of the 2-(2-Hydroxyaryl)-1,3,5-triazine class and their methoxy derivatives: fluorescence spectroscopy and x-ray structure analysis. *J Phys Chem A* 102:6975–6985
- Martinej ML, Cooper WC, Chou PT (1992) A novel excited-state intramolecular proton transfer molecule, 10-hydroxybenzo[h]quinoline. *Chem Phys Lett* 193:151–154
- Wu Y, Peng X, Fan J, Gao S, Tian M, Zhao J, Sun S (2007) Fluorescence sensing of anions based on inhibition of excited-state intramolecular proton transfer. *J Org Chem* 72:62–70
- Shah M, Thangaraj K, Soong ML, Wolford LT, Boyer JH, Politzer IR, Pavlopoulos TG (1990) Pyrromethene-BF<sub>2</sub> complexes as laser dyes. Part I. *Heteroat Chem* 1:389–399
- Paviopoulos TG, Boyer JH, Thangaraj K, Sathyamoorthi G, Shah MP, Soong ML (1992) Laser dye spectroscopy of some pyrromethene-BF<sub>2</sub> complexes. *Appl Opt* 31:7089–7094
- Costela A, Garcia-Moreno I, Gomez C, Sastre R, Amat-Guerri F, Liras M, Lopez Arbeloa F, Banuelos Prieto J, Lopez Arbeloa I (2002) Photophysical and lasing properties of new analogs of the boron-dipyrromethene laser dye PM567 in liquid solution. *J Phys Chem A* 106:7736–7742
- Lopez Arbeloa F, Ruiz Ojeda P, Lopez Arbeloa I (1988) On the aggregation of rhodamine B in ethanol. *Chem Phys Lett* 148:253–258
- Rahn MD, King TA, Gorman AA, Hamblett I (1997) Photostability enhancement of pyrromethene 567 and perylene orange in oxygen-free liquid and solid dye lasers. *Appl Opt* 36:5862–5871
- Assor Y, Burshtein Z, Rosenwaks S (1998) Spectroscopy and laser characteristics of copper-vapor-laser pumped pyrromethene-556 and pyrromethene-567 dye solutions. *Appl Opt* 37:4914–4920
- Costela A, Garcia-Moreno I, Sastre R (2001) In: Nalwa HS (ed) *Handbook of advanced electronic and photonic materials and devices*. Academic, San Diego, p 7, 161
- O'Neil MP (1993) Synchronously pumped visible laser dye with twice the efficiency of Rhodamine 6 G. *Opt Lett* 18:37–38
- Rhan MD, King TA (1995) Comparison of laser performance of dye molecules in sol-gel, polycom, ormosil, and poly(methyl methacrylate) host media. *Appl Opt* 34:8260–8271

21. Dubois A, Canva M, Brun A, Chaput F, Boilot JP (1996) Photostability of dye molecules trapped in solid matrices. *Appl Opt* 35:3193–3199
22. Yariv E, Schultheiss S, Saraidarov T, Reisfeld R (2001) Efficiency and photostability of dye doped solid state lasers in different hosts. *Opt Mater (Amsterdam)* 16:29–38
23. Lopez Arbeloa F, Lopez Arbeloa I, Lopez Arbeloa T (2001) In: Nalwa HS (ed) *Handbook of advanced electronic and photonic materials and devices*. Academic, San Diego, p 7, 209
24. Jayabharathi J, Thanikachalam V, Srinivasan N, Saravanan K (2010) Synthesis, structure, luminescent and intramolecular proton transfer in some imidazole derivatives. *J Fluoresc*. doi:10.1007/s10895-010-0747-5
25. Yamada M, Tanaka Y, Yoshimoto Y, Kuroda S, Shimo I (1992) Synthesis and properties of diamino-substituted dipyrro [3,2-*a*:2',3'-*c*]phenazine. *Bull Chem Soc Jpn* 65:1006–1011
26. Jayabharathi J, Thanikachalam V, Saravanan K, Srinivasan N (2010) Iridium(III) complexes with orthometalated imidazole ligands subtle turning of emission to the saturated green colour. *J Fluoresc*. doi:10.1007/s10895-010-0737-7
27. Saravanan K, Srinivasan N, Thanikachalam V, Jayabharathi J (2010) Synthesis and photophysics of some novel imidazole derivatives used as sensitive fluorescent chemisensors. *J Fluoresc* 21:65–80
28. Gayathri P, Jayabharathi J, Srinivasan N, Thiruvalluvar A, Butcher RJ (2010) 2-(4-Fluorophenyl)-4,5-dimethyl-1-(4-methylphenyl)-1H-imidazole. *Acta Crystallogr E* 66:o1703
29. Jayabharathi J, Thanikachalam V, Venkatesh Perumal M, Saravanan K (2011) Displacement reaction using ibuprofen in a mixture of bioactive imidazole derivative and bovine serum albumin – a fluorescence quenching study. *J Fluoresc*. doi:10.1007/s10895-011-0878-3
30. Jayabharathi J, Thanikachalam V, Venkatesh Perumal M, Srinivasan N (2011) Fluorescence resonance energy transfer from a bio-active imidazole derivative 2-(1-phenyl-1H-imidazo[4,5-*f*][1, 10]phenanthroline-2-yl)phenol to a bioactive indoloquinone lizine system. *Spectrochim Acta A* 79:236–244
31. Jayabharathi J, Thanikachalam V, Saravanan K, Srinivasan N, Venkatesh Perumal M (2010) Physicochemical properties of organic nonlinear optical crystal from a combined experimental and theoretical study. *Spectrochim Acta A* 78:794–802
32. Jayabharathi J, Thanikachalam V, Jayamoorthy K, Venkatesh Perumal M (2011) Physicochemical studies of excited state intramolecular proton transfer process Luminescent chemosensor by spectroscopic investigation supported by ab initio calculations. *Spectrochim Acta A* 79:6–16
33. Gayathri P, Jayabharathi J, Srinivasan N, Thiruvalluvar A, Butcher RJ (2010) 4,5-Dimethyl-2-phenyl-1-(*p*-tolyl)-1H-imidazole. *Acta Crystallogr E* 66:o2826
34. Jayabharathi J, Thanikachalam V, Saravanan K (2009) Effect of substituents on the photoluminescence performance of Ir(III) complexes: Synthesis, electrochemistry and photophysical properties. *J Photochem Photobiol A: Chem* 208:13–20
35. Gaussian 03 program, (Gaussian Inc., Wallingford CT) (2004)
36. Banuelos Prieto J, Lopez Arbeloa F, Virginia Martinez Martinez T, Lopez A, Lopez Arbeloa I (2004) Photophysical properties of the pyrromethene 597 dye: solvent effect. *J Phys Chem A* 108:5503–5508
37. Hofer JE, Grabenstetter RJ, Wiig EO (1950) The fluorescence of cyanine and related dyes in the monomeric state. *J Am Chem Soc* 72:203–209
38. Lopez Arbeloa I (1980) Fluorescence quantum yield evaluation. Reabsorption and reemission corrections. *J Photochem* 14:97–105
39. Bergstrom F, Mikhalyov I, Hagglof P, Wortmann R, Ny T (2002) Dimers of dipyrrometheneboron difluoride (BODIPY) with light spectroscopic applications in chemistry and biology. *J Am Chem Soc* 124:196–204
40. Marcus Y (1993) The properties of organic liquids that are relevant to their use as solvating solvents. *Chem Soc Rev* 22:409–416
41. Reichardt C (1994) Solvatochromic dyes as solvent polarity indicators. *Chem Rev* 94:2319–2358
42. Catalan J (1997) On the E(T) (30), pi, P(y), S', and SPP empirical scales as descriptors of nonspecific solvent effects. *J Org Chem* 62:8231–8234
43. Lippert E (1975) In: Birks JB (ed) *Organic molecular photophysics*. Wiley-Interscience, Bristol, p 2, 1
44. Dimroth K, Reichardt C (1969) Of pyridinium *N*-phenol betaines and their use for characterizing the polarity of solvents, V Expansion of the solvent polarity scale by using alkyl-substituted pyridinium *N*-phenol betaines. *Liebigs Ann Chem* 727:93–105
45. Kamlet MJ, Taft RW (1976) The solvatochromic comparison method. I. The  $\beta$ -scale of solvent hydrogen-bond acceptor (HBA) basicities. *J Am Chem Soc* 98:377–383
46. Catalan J, Lopez V, Perez P (1996) Use of the SPP scale for the analysis of molecular systems with dual emissions resulting from the solvent polarity. *J Fluoresc* 6:15–22
47. Dunsbach R, Schmidt R (1994) Photophysical properties of some polycyclic conjugated hydrocarbons containing five membered rings. *J Photochem Photobiol A* 83:7–13
48. Biczok L, Berces T, Marta F (1993) Substituent, solvent, and temperature effects on radiative and nonradiative processes of singlet excited fluorenone derivatives. *J Phys Chem* 97:8895–8899
49. Andersson PO, Bachilo SM, Chen RL, Gillbro T (1995) Solvent and temperature effects on dual fluorescence in a series of carotenes. Energy gap dependence of the internal conversion rate. *J Phys Chem* 99:16199–16209
50. Carvalho CEM, Brinn IM, Pinto AV, Pinto MCFR (2000) Fluorescent symmetric phenazines from naphthoquinones. 3. Steady state spectroscopy and solvent effect of seven phenazine derivatives: structure-photophysics correlations. *J Photochem Photobiol A* 136:25–33
51. Drexhage KH (1990) Dye lasers topics. In: Schafer FP (ed) *Topics in applied physics*, 1. Springer, Berlin, p 187
52. Birks JB (1970) *Photophysics of aromatic molecules*. Wiley-Interscience, London
53. Allik T, Chandra S, Robinson TR, Hutchinson JA, Sathyamoorthi G, Boyer JH (1994) Laser performance and material properties of a high temperature plastic doped with pyrromethene-BF2 dyes. *Mater Res Soc* 329:291–296
54. He GS, Prasad PN (1998) Phase-conjugation property of one-photon pumped backward stimulated emission from a lasing medium. *J Quant Electron* 34:473–481
55. Yariv E, Reisfeld R (1999) Laser properties of pyrromethene dyes in sol gel glasses. *J Opt Mater* 13:49–54
56. Finlayson AJ, Peters N, Kolinsky PV, Venner RW (1999) Flashlamp pumped solid-state dye laser incorporating pyrromethene 597. *Appl Phys Lett* 75:457–459